Available online at www.sciencedirect.com

ScienceDirect

Proceedings of the Combustion Institute 38 (2021) 3427–3434

Proceedings of the Combustion Institute

www.elsevier.com/locate/proci

Large-eddy simulation of n-dodecane spray flame: Effects of nozzle diameters on autoignition at varying ambient temperatures

Jiun Cai Ong [a], Kar Mun Pang [b,*], Xue-Song Bai [c], Mehdi Jangi [d], Jens Honore Walther [a,e]

[a] *Department of Mechanical Engineering, Technical University of Denmark, 2800 Kgs. Lyngby, Denmark*
[b] *MAN Energy Solutions, Teglholmsgade 41, 2450 København SV, Denmark*
[c] *Department of Energy Sciences, Lund University, 22100 Lund, Sweden*
[d] *Department of Mechanical Engineering, University of Birmingham, Birmingham, B15 2TT, UK*
[e] *Computational Science and Engineering Laboratory, ETH Zürich, CH-8092 Zürich, Switzerland*

Received 6 November 2019; accepted 11 August 2020
Available online 14 October 2020

Abstract

In the present study, large-eddy simulations (LES) are used to identify the underlying mechanism that governs the ignition phenomena of spray flames from different nozzle diameters when the ambient temperature (T_{am}) varies. Two nozzle sizes of 90μm and 186μm are chosen. They correspond to the nozzle sizes used by Spray A and Spray D, respectively, in the Engine Combustion Network. LES studies of both nozzles are performed at three T_{am} of 800K, 900K, and 1000K. The numerical models are validated using the experimental liquid and vapor penetration, mixture fraction (Z) distribution, as well as ignition delay time (IDT). The ignition characteristics of both Spray A and Spray D are well predicted, with a maximum relative difference of 14% as compared to the experiments. The simulations also predict the annular ignition sites for Spray D at $T_{am} \geqslant 900$K, which is consistent with the experimental observation. It is found that the mixture with $Z \leqslant 0.2$ at the spray periphery is more favorable for ignition to occur than the overly fuel-rich mixture of $Z > 0.2$ formed in the core of spray. This leads to the annular ignition sites at higher T_{am}. Significantly longer IDT for Spray D is obtained at T_{am} of 800K due to higher scalar dissipation rates (χ) during high temperature (HT) ignition. The maximum χ during HT ignition for Spray D is larger than that in Spray A by approximately a factor of 5. In contrast, at $T_{am} = 1000$K, the χ values are similar between Spray A and Spray D. This elucidates the increase in the difference of IDT between Spray D and Spray A as T_{am} decreases. This may explain the contradicting findings on the effects of nozzle diameters on IDT from literature.

Keywords: Spray A; Spray D; Autoignition; Nozzle Size; LES

* Corresponding author.
E-mail address: kar.pang@man-es.com (K.M. Pang).

https://doi.org/10.1016/j.proci.2020.08.018

1. Introduction

Understanding the ignition characteristics of diesel spray combustion is critical as a longer ignition delay time (IDT) increases the local premixing, thus reducing emission [1,2]. Different nozzle diameter sizes (D_{noz}) show significantly different effects on the ignition characteristics in diesel engines [7,3–6]. Decreasing D_{noz} was shown to reduce the IDT [7,3]. At the same time, other studies [4–6] showed contradicting findings, where varying the D_{noz} had no significant effects on the IDT in a diesel engine. It is worth mentioning that in-cylinder flow varies from one engine to another due to different piston bowl and intake valves configurations. The injection characteristics were also not standardized. Hence, the air-fuel mixing is expected to vary as well. These collectively make direct comparison of the results from different diesel engine data difficult.

To better understand the effects of D_{noz} on ignition characteristics without the complex in-cylinder flow, experimental studies were carried out in a constant volume vessel with controlled ambient pressure and temperature conditions which resemble those of direct injection diesel engines. One of the earliest works on investigating different D_{noz} for diesel spray combustion was carried out by Sieber and Higgins [8,9] using the grade number two diesel fuel (diesel #2). IDTs from four D_{noz} of 100μm, 180μm, 246μm, and 363μm at varying ambient temperatures (T_{am}) from 800K–1200K are available on ECN [9]. The work focused on the effects of D_{noz} on flame stabilization. Revisiting the associated IDTs in the study reveals a non-monotonic trend when D_{noz} varies. At $T_{am} \geqslant 900$K, varying D_{noz} have no significant effects on IDT. However, at 800K, the IDTs exhibit a non-monotonic trend where $IDT_{180\mu m} < IDT_{100\mu m} < IDT_{246\mu m}$. Thereafter, a great amount of experimental and numerical effort was placed in studying Spray A in the Engine Combustion Network (ECN) [9], which uses *n*-dodecane fuel ($C_{12}H_{26}$) and a D_{noz} of 90μm. The baseline ambient conditions are standardized to a T_{am} of 900K, gas density (ρ_{am}) of 22.8kg/m^3, and molar oxygen concentration ($O_{2,am}$) of 15%.

Recently, Spray D configuration is introduced by ECN, which has the same ambient conditions and fuel type as Spray A, but uses an injector that has approximately twice the size of the nominal D_{noz} of Spray A. Experimental studies on ignition and combustion characteristics of Spray D were performed by Westlye [10] and Pastor et al. [11]. The IDT measurement of Spray A and Spray D took into account the hydraulic delay during fuel injection and were based on natural luminosity from the flame. Different T_{am}, $O_{2,am}$ and injection pressures (P_{inj}) were varied in their experimental studies. Spray D was shown to have a longer IDT than Spray A across different T_{am} [11]. The slower mixing in Spray D was suggested to be the main reason for this observation [11]. The experimental studies also showed that the differences in IDTs between Spray D and Spray A were increasing as T_{am} decreases. The physics behind this was, however, not clearly addressed in the paper.

From a simulation point of view, Pang et al. [12] performed a three-dimensional, computational fluid dynamics (CFD) study on reacting sprays in a constant volume combustion vessel with D_{noz} of 100μm, 180μm, and 363μm. The simulations were carried out by coupling unsteady Reynolds-averaged Navier-Stokes with an Eulerian Stochastic Field method [12]. Their results were consistent with experimental observation, which showed no significant effect on IDT across the three D_{noz} at T_{am} of 1000K. Comparison of Spray D and Spray A was carried out in the numerical study by Desantes et al. [13]. It was shown that a reduction in D_{noz} promotes faster mixing which shortens the time needed to reach ignitable equivalence ratio, therefore shorter IDT. All the numerical works mentioned above for different D_{noz} were only performed at a single T_{am}. On the other hand, comprehensive studies of the effects of T_{am} on ignition and spray flame were carried out by Pei et al. [14] and Pang et al. [15]. However, the works were carried out only for small D_{noz}. Therefore, the coupled effects between D_{noz} and T_{am} on ignition characteristics are still not well understood.

Set against these backgrounds, this paper first aims to identify the underlying mechanism that controls the ignition process of spray flame from different D_{noz} at varying T_{am}. Further emphasis is placed on understanding the experimentally observed increasing difference of IDTs between Spray D and Spray A as T_{am} decreases. Moreover, this work also aims to resolve the contradicting findings on the effects of D_{noz} on IDT from literature. These aims are achieved by performing large-eddy simulations (LES) of Spray A and Spray D at T_{am} of 800K, 900K, and 1000K.

2. Numerical methods and case setup

The present LES is performed using OpenFOAM-v1712. The Eulerian-Lagrangian approach is used within the LES framework for spray modeling. The gas phase is described using spatially filtered transport equations. Both temporal and spatial terms are discretized using implicit second-order schemes. The sub-grid scale (SGS) is modeled using the Dynamic *k*-equation. The pressure-velocity coupling is implemented in terms of the Pressure Implicit with Splitting of Operator (PISO) algorithm. The injected liquid phase of $C_{12}H_{26}$ is modeled as discrete parcels whose motion is described using the Lagrangian particle tracking approach. Each parcel represents a group of spher-

ical droplets whose position, size, and physical properties are similar. The primary breakup is considered by injecting computational parcels with the Rosin-Rammler distribution of size ranging from $0.1 \times D_{noz}$ to D_{noz}. The secondary breakup is modeled by Reitz-Diwakar spray model, where the stripping breakup constant, C_s is set to 10 [16]. The spray half-angle for all cases is set to 10°. The Frossling model and the Ranz-Marshall correlation are employed to account for the droplet evaporation and heat transfer with the surrounding gas phase, respectively.

The skeletal $C_{12}H_{26}$ mechanism developed by Yao et al. [17] (54 species and 269 reactions) is used in this work. The mechanism has shown good performance in the spray combustion context [18,19]. Tabulated models were successfully applied in LES of Spray A combustion across numerous operating conditions [20,21]. While the tabulated models are highly efficient, special care is required when the look-up table is constructed, which is only reliable within a narrower range of specific operating conditions. Thus, a general, direct chemistry coupling approach is preferred in this study. The well-stirred reactor (WSR) model is successfully used in simulating Spray A [14,19], but it does not consider turbulence-chemistry interaction (TCI). The partially-stirred reactor (PaSR) [22] combustion model is hence used here to account for the TCI effects. The C_{mix} value in the PaSR model is set to 0.3 and used throughout all reactive spray cases. A sensitivity study is performed and within a 10% change in IDT is found when the C_{mix} value decreases from 0.3 to 0.03. The Chemistry Coordinate Mapping (CCM) approach is coupled with the PaSR model in order to speed up the integration process of the chemical reaction rates [23]. This method has been successfully implemented to LES of spray combustion [24]. More details about the CCM approach are available in [15,23].

The experimental reference case for the simulations in the current study corresponds to ECN Spray A ($D_{noz} = 90\mu m$) and Spray D ($D_{noz} = 186\mu m$) baseline conditions [9]. Both Spray A and Spray D have the same P_{inj} of 1500bar, fuel temperature of 363K and ρ_{am} of 22.8kg/m^3. The rate of injection from ECN [9] with an averaged fuel mass flow rate of 2.295g/s is used for Spray A, while a top hat injection profile with an averaged fuel mass flow rate of 11.71g/s [10] is used for Spray D. The operating conditions and the fuel injection are summarized in Table 1, where $\dot{m}_f$ denotes the injected fuel mass flow rate. Cases 1–4 are Spray A cases; while cases 5–8 are Spray D cases. Cases 1 and 5 are inert spray cases, where the $O_{2,am}$ is set to zero. The ambient mixture composition and temperature are initiated as uniform field while the velocity field is set to zero. Details of the ambient composition can be found in [9]. The computational domain is a constant volume cubic chamber with side lengths of 108mm. All boundaries are set as no-slip, adiabatic wall. The injector is placed at the center of one of the chamber walls. A uniform mesh of 0.125mm is used within the spray combustion region (80mm axially and 15mm radially from the nozzle location) and a coarser mesh resolution is used outside the spray combustion region. This mesh resolution is the same as those reported in [14,25]. A grid sensitivity study can also be found in the Supplemental material S1. The current setup is shown in Section 3 to accurately capture the penetration lengths, mixture fraction profiles, and IDT.

Table 1
Operating conditions and injector specifications

Case	$O_{2,am}$ [% mol]	T_{am} [K]	D_{noz} [μm]	$\dot{m}_f$ [g/s]
1	0	900	90	2.295
2	15	800	90	2.295
3	15	900	90	2.295
4	15	1000	90	2.295
5	0	900	186	11.71
6	15	800	186	11.71
7	15	900	186	11.71
8	15	1000	186	11.71

3. Validation of models

3.1. Inert spray

While validation of LES using Spray A data can be widely found in the literature, those using Spray D are scarcely found to the best of the authors' knowledge. The validation of the computational setup is carried out by comparing the liquid penetration length (LPL), vapor penetration length (VPL), and the radial mixture fraction profiles at two axial positions with the experimental data of ECN [9]. LPL is defined as the maximum axial location from the injector to the location where 95% of the total liquid mass is found; VPL is determined using the farthest downstream location of 0.1% fuel mass fraction. The test conditions for the inert spray validation of Spray A and Spray D correspond to Case 1 and Case 5, respectively, in Table 1.

Figure 1a shows the comparison of simulated LPL and VPL against the measurements. It is important to note that the same numerical configurations are used in both Spray A and Spray D simulations. Without calibrating any other model constant for each spray, the predicted penetration lengths for Spray A and Spray D are in good agreement with the experimental data. The sensitivity study of T_{am} on LPL and VPL for both Spray A and Spray D are available in the Supplemental material S2.

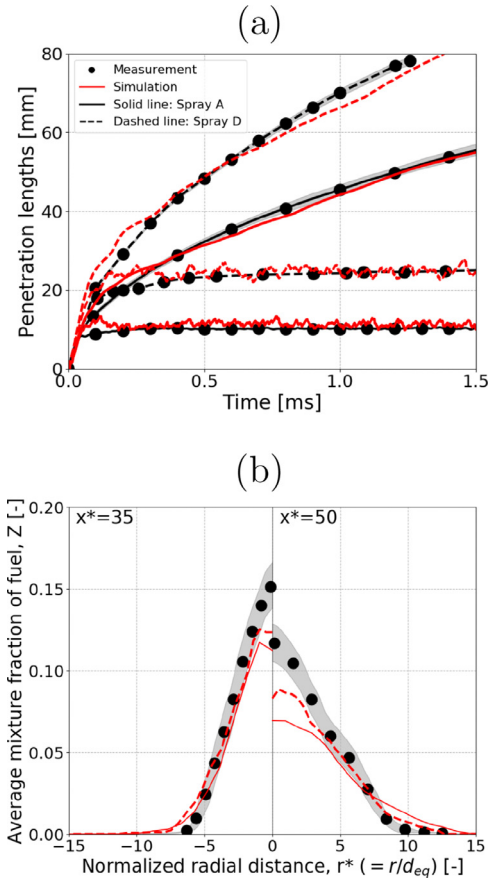

Fig. 1. (a) Penetration lengths of liquid and vapor fuel for Spray A (solid-lines) and Spray D (dashed-lines). (b) Average mixture fraction distribution along normalized radial direction, r^* at normalized axial distance, $x^* = 35$ and 50. The gray shadow represents the error bar of 95% confidence interval for the measurements.

In addition, mixture fraction (Z) fields of Spray A and Spray D are compared with the experimental data in Fig. 1b in normalized radial (r^*) and axial (x^*) coordinates. The experimental data shown in Fig. 1b is for inert Spray A which was performed through Rayleigh Scattering throughout the injection period, in which the images taken were then converted to Z [9]. The normalized coordinates r^* and x^* are computed by normalizing the radial (r) and axial coordinate (x) by the equivalent diameter (d_{eq}) of each nozzle, i.e., $r^* = r/d_{eq}$ and $x^* = x/d_{eq}$ [11,13]. The equivalent diameter is calculated as $d_{eq} = D_{noz}\sqrt{\rho_f/\rho_{am}}$, where ρ_f denotes the density of fuel. It is shown in [11,13] that the Z profiles for Spray A and Spray D collapse onto one another in normalized coordinates. It is hence possible to compare the Z fields for Spray A and Spray D against the experimental data for Spray A. The Z profiles are obtained from a single LES realization

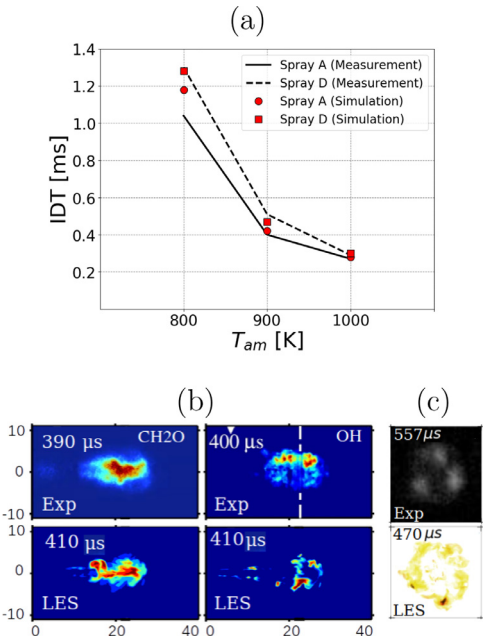

Fig. 2. (a) The IDTs for the LES cases at different T_{am}. Lines - measurement data. Symbols - simulation result. (b) Comparison of CH_2O and OH distributions from PLIF measurements [9,27] (top) and LES calculations (bottom) at IDT for Spray A at $T_{am} = 900$K. Spatial units in mm. (c) Comparison of measured broadband luminosity images [11] (top) and simulated instantaneous isovolume of OH mass fraction ($OH \geqslant 2\%(OH_{max})$) (bottom) at $T_{am} = 900$K after IDT of Spray D from the frontal viewing angle. OH_{max} is fixed at 5×10^{-5}. Each frame shows 20 mm $\times$ 20 mm.

by time averaging from 1.5 to 2ms. An additional spatial averaging is performed in the circumferential direction. As shown in Fig. 1b, the model shows good qualitative agreement for both Spray A and Spray D at $x^* = 35$ and 50 for $|r^*| \geqslant 2$. The underprediction close to the spray centerline can be improved by increasing the spatial resolution [26] but that leads to a much higher computational cost. Considering that the current computational setup achieves a balance between accuracy and computational efficiency, the same setup is used next in simulating the reacting spray cases.

3.2. Reacting spray

In the following analysis, the IDTs for Spray A and Spray D at different T_{am} are simulated and compared against the measurements, as shown in Fig. 2a. The computed IDTs have the same definition as the measurements, which is the time from start of injection to the time when the maximum rate of maximum temperature rise in the domain occurs [14]. This definition is in accordance to the ECN recommendation [9]. The larger discrepancy at $T_{am} = 800$K in Fig. 2a may be attributed to

the simplification of the lumped low temperature oxidation sub-mechanism [17]. Despite this, the predicted IDTs across different T_{am} and D_{noz} has a maximum relative difference of 14% compared to the measurements. Figure 2a also depicts that the predicted IDT for Spray D is shown to be longer than Spray A across the three T_{am}, where the largest deviation is at 800K. This observation corresponds to the findings in [11]. Additional information about the performance of Yao mechanism as compared to another reduced mechanism is available in the Supplemental material S3.

Further validation is performed to assess the model performance in predicting intermediate species. The instantaneous mass fraction distributions of important intermediate combustion product, such as formaldehyde (CH_2O) and hydroxyl (OH) at IDT for Spray A at $T_{am} = 900$K are compared against the measurements obtained from planar laser induced fluorescence (PLIF) [9,27]. It can be seen from Fig. 2b that a good qualitative agreement between LES and measurements is obtained for the spatial distribution of CH_2O and OH. Moreover, Fig. 2c compares the instantaneous iso-volume of OH after IDT for Spray D at T_{am} of 900K, which shows that the high temperature (HT) regions are at the spray periphery. This corresponds to the annular ignition pattern shown in the Spray D experiment [11].

4. Results and discussion

In this section, the ignition characteristics obtained from LES of Spray A and Spray D at T_{am} of 1000K and 800K are investigated and compared. For all four cases (Case 2, 4, 6, and 8 in Table 1), the 1st-stage ignition first initiates in the fuel-lean region ($Z < Z_{st}$), where Z_{st} is the stoichiometric mixture fraction with a value of 0.045 [14]. It is followed by an apparent temperature rise within the fuel-rich region ($Z > Z_{st}$). Thereafter, the HT combustion occurs within a relatively less-rich mixture. These observations agree with the findings from LES simulations by Pei et al. [14]. However, the associated spatial distribution of intermediate species (e.g. CH_2O) as well as the ignition location are different between Spray A and Spray D. Mass fraction of dodecyl peroxide radicals, $C_{12}H_{25}O_2$ (RO_2 is henceforth used for brevity) is often used as an indicator for the 1st-stage ignition activity [28] as it is one of the important species in the decomposition pathway of $C_{12}H_{26}$. Therefore, the spatial distributions of both RO_2 and CH_2O are considered in the following analysis.

4.1. Ignition characteristics at high T_{am} ($T_{am} = 1000K$)

Figure 3 illustrates the temporal evolution of reacting spray at 1000K for Spray A (Fig. 3a–c) and Spray D (Fig. 3d–f). At 0.18ms (after the 1st-stage ignition occurs), a significant amount of CH_2O is observed downstream ($x > 10$mm) of Spray A, while a significant amount of RO_2 is only present at the upstream region just after the liquid spray (cf. Fig. 3a). At 0.22ms, the concentration of CH_2O at the head of the spray has decreased, while a high concentration of CH_2O remains upstream of the spray, at the end of the liquid spray. From 0.22ms to 0.28ms, Fig. 3b depicts that the reacting spray tip region of Spray A has multiple ignition sites ($\Delta T > 400$K). These ignition sites subsequently spread to the whole spray head as shown in Fig. 3c. This location coincides with the igni-

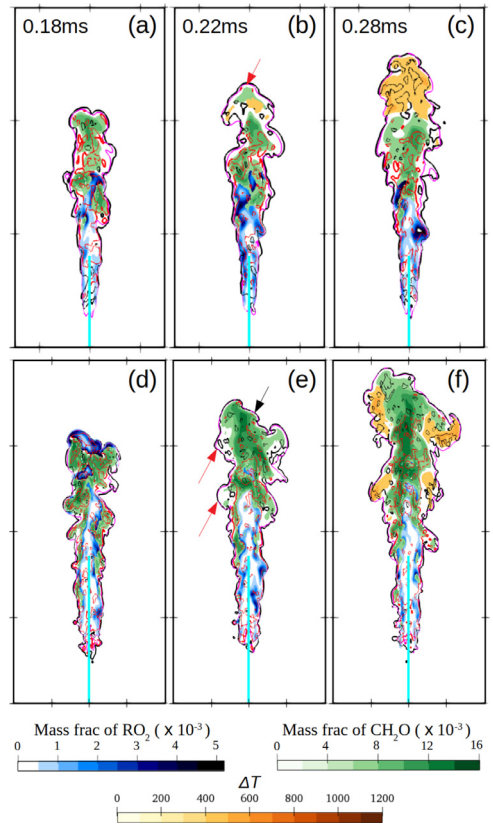

Fig. 3. The temporal evolution of RO_2, CH_2O, and ΔT fields at 1000K for Spray A (a–c) and Spray D (d–f). ΔT is defined as the change of temperature relative to T_{am}. The stoichiometric mixture fraction, Z_{st} is shown by magenta solid line. The scalar dissipation rates, χ of $10s^{-1}$ and $1s^{-1}$ are represented by red solid line and black solid line, respectively. Solid cyan line indicates the averaged liquid length. The range considered for the iso-surface of RO_2 is 1×10^{-4} and 5×10^{-3}; for CH_2O is 6×10^{-3} and 16×10^{-3}; and for ΔT to be 400K and 1200K. Red arrow indicates HT ignition. Black arrow indicates no ignition. For a–c, each frame above shows 15mm × 30mm; whereas for d–f, each frame above shows 20mm × 40mm.

tion region observed experimentally in [9]. Furthermore, the predicted ignition sites occur in regions where the scalar dissipation rates, χ, are less than $10s^{-1}$, which agrees well with the findings in [29]. On the other hand, Spray D exhibits a different ignition characteristics than Spray A. At 0.18ms, RO_2 and CH_2O co-exist in the spray head region as shown in Fig. 3d. The high concentration of RO_2 at the spray head indicates that the fuel is decomposing to RO_2. At a subsequent time ($t = 0.22$ms), most of the RO_2 has decomposed into intermediate species, such as CH_2O. Hence, a high concentration of CH_2O is present downstream of the spray, while RO_2 is only present upstream of the spray. At 0.22ms, the χ values at both the spray head (indicated by black arrow) and the peripheral region (indicated by red arrows) are equally low ($< 10s^{-1}$), as shown in Fig. 3e. It is also worth mentioning that the local temperature in both regions are approximately 1400K. However, only the mixture at the periphery of the spray undergoes HT ignition (cf. Fig. 3f). This can be explained by examining the Z at both the central and peripheral region of the spray (figures are available in the Supplemental material S4).

The spray center region of Spray D has a fuel-rich mixture of $Z > 0.2$. In contrast, the periphery of the spray, where the HT ignition occurs, has a mixture of $Z \leqslant 0.2$. It indicates that overly fuel-rich ($Z > 0.2$) regions are unfavorable for ignition despite having a low χ and a temperature of approximately 400K above T_{am}. Hence, the periphery of the spray, which has a low χ value and $Z \leqslant 0.2$, becomes the most favorable location for ignition. This observation is supported by the findings from the two-dimensional (2D) direct numerical simulation (DNS) conducted by Krisman et al. [30]. It is shown that a cool-flame takes a longer time to reach the most fuel-rich mixture [30]. Meanwhile, the fuel-rich mixture itself takes a longer time to have spontaneous ignition due to having a longer low temperature IDT [31]. Both these reasons lead to the core region of the spray jet, which has a fuel-rich mixture, to have a slower low temperature reaction than at the spray periphery, which is more fuel-lean. As a result, the HT ignition occurs at the spray periphery. It is noteworthy that the ignition at the spray periphery is akin to the observation at 900K in Fig. 2c as discussed in Section 3.2. Furthermore, the HT regions from the spray periphery converge at the spray head at approximately 0.1ms after IDT.

4.2. *Ignition characteristics at low* T_{am} ($T_{am} = 800K$)

The ignition characteristics for low T_{am} are illustrated in Fig. 4. For Spray A in particular, some similarities in the temporal evolution of reacting spray can be observed between the 800K and 1000K case. Before 1.0ms (not shown), a small

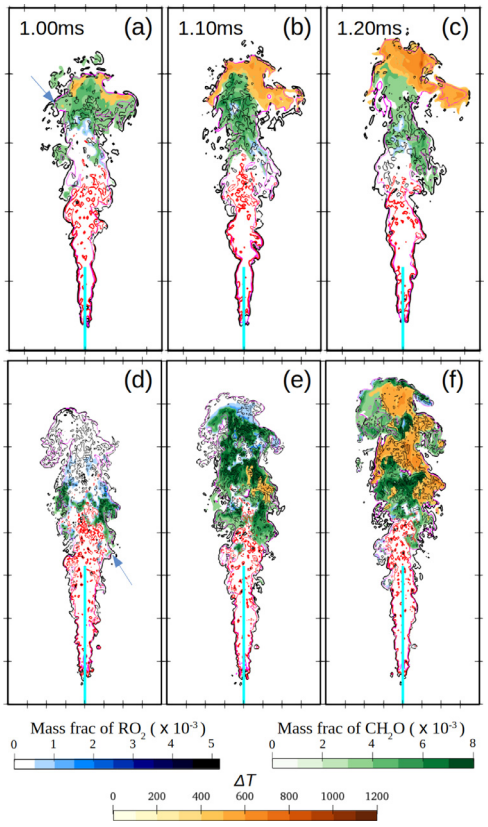

Fig. 4. The temporal evolution of RO_2, CH_2O, and ΔT fields at 800K for Spray A (a–c) and Spray D (d–f). The scalar dissipation rates, χ of $1s^{-1}$ and $0.1s^{-1}$ are represented by red solid line and black solid line, respectively. The range considered for the iso-surface of CH_2O is 3×10^{-3} and 16×10^{-3}. Other information and descriptions can be found in the caption of Fig. 3. Blue arrow indicates 1st-stage ignition. For a–c, each frame above shows 25mm × 50mm; whereas for d–f, each frame above shows 40mm × 80mm.

amount of RO_2 is initially formed at the spray head (indicated by the blue arrow in Fig. 4a) and the ignition kernels subsequently propagate to the whole frontal region of the spray. As such, a high concentration of CH_2O is seen at the spray head in Fig. 4a at 1.0ms. Meanwhile, regions of $\Delta T > 400$K start to appear at the tip of the spray head where the local χ value is less than $1s^{-1}$. It is noteworthy that the χ value is an order of magnitude lower than that in the 1000K case. In subsequent time frames (Fig. 4b and c), the HT region starts to propagate throughout the spray head and a higher temperature is attained. This trend is similarly obtained in [29] for Spray A at $T_{am} = 750$K.

The ignition phenomenon of Spray D is different from Spray A, as depicted in Fig. 4d–f. At 1.0ms (not shown), the onset location of the 1st-

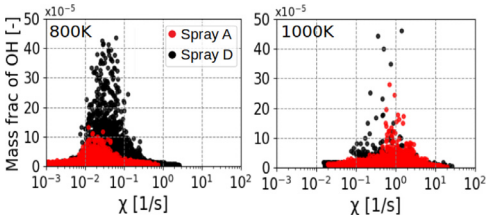

Fig. 5. Scatter plots of mass fraction of OH and scalar dissipation rates, χ for Spray A and Spray D at their respective IDTs. Left: $T_{am} = 800$K. Right: $T_{am} = 1000$K.

stage ignition for Spray D occurs at the spray periphery (indicated by the blue arrow in Fig. 4d) but not at the spray head as in Spray A. Furthermore, the 1st-stage ignition takes place in the vicinity of the spray core region where the cold, fuel-rich mixture prohibits ignition to occur. Hence, the ignition kernel can only propagate downstream along the side of the spray as shown in Fig. 4d ($t = 1.0$ms). At this time instance, the formation of CH_2O occurs at the side of the spray, but not at the spray head. Only until 1.1ms, a significant amount of CH_2O and RO_2 are present at the spray head as shown in Fig. 4e. Meanwhile, ignition sites where $\Delta T > 400$K start to form at the periphery of the spray and slowly propagate toward the center region. As more ignition sites are formed at the side of the spray and even at the spray head, a volumetric ignition process can be observed in Fig. 4f. The co-existence of the cool-flame (which is indicated by CH_2O) and the HT ignition at $T_{am} = 800$K for both D_{noz} agrees with the 2D DNS results shown by Krisman et. al. [30]. One should also note that the annular ignition pattern seen in the previous section is not observed in this low T_{am} case. This implies that the annular pattern is only profound at high T_{am} where the associated chemical time scale is shorter and the ignition sites fall closer to the liquid fuel.

Figure 4 illustrates that Spray D takes a longer time to achieve HT ignition than Spray A for the same time instances (cf. Fig. 4). This can be attributed to the difference in χ between Spray D and Spray A. Figure 5 shows the scatter plot of OH and χ for Spray A and Spray D at their respective IDTs. At 800K, the maximum χ in Spray D is higher than in Spray A by approximately a factor of 5. A high χ leads to longer IDT [31], hence explaining the longer IDT obtained in Spray D than in Spray A. On the other hand, at 1000K, the OH-χ distribution of Spray A and Spray D coincides with each other. Thus, indicating that the IDT for the 1000K cases will be similar. This result corresponds with the observation in Section 3 and the experiment [11], which shows that the difference of IDT between Spray D and Spray A increases as T_{am} decreases.

5. Conclusion

The present work implements LES with a finite-rate chemistry to study the coupled effects of T_{am} and D_{noz}. The LES model captures the key characteristics of different D_{noz} of 90μm (Spray A) and 186μm (Spray D) at T_{am} of 800K, 900K, and 1000K. The LPL, VPL, and radial Z profiles are well predicted as compared to the measurements. Moreover, the IDTs predicted are within a maximum relative difference of 14% as compared to the measurements across different T_{am} and D_{noz}.

At $T_{am} = 1000$K, both experiment and LES show comparable IDTs between Spray A and Spray D. The numerical results show that the χ and thermochemical conditions prior to HT ignition are both similar. The local Z, however, strongly influences the ignition pattern. The HT ignition site for Spray A occurs at the spray head, whereas it occurs at the periphery of the spray in Spray D. The ignition process in Spray D leads to an annular ignition pattern, which was demonstrated experimentally and replicated in the present LES study. Despite having a maximum temperature of 400K above T_{am} at the center region of the spray head, the current result suggests that the mixture is unfavorable for ignition due to having fuel-richer mixture ($Z > 0.2$). Instead, the ignition occurs at the periphery of the spray where $Z \leqslant 0.2$. The annular pattern of ignition sites is observed at $T_{am} \geqslant 900$K, where the associated chemical time scale is shorter and the ignition sites fall closer to the liquid fuel.

At $T_{am} = 800$K, the IDT is longer for Spray D, which is replicated in the LES. While the thermochemical conditions are similar in these two cases, the maximum χ for Spray D is higher than that in Spray A by approximately a factor of 5. The lower χ is found to be the main factor that leads to the larger difference in IDT between Spray A and Spray D. It is also noted that the χ values at 800K are an order of magnitude lower than those at 1000K, regardless of D_{noz}.

This work assists to explain the increase in the difference of IDT between Spray D and Spray A as T_{am} decreases, and also to shed light on the contradicting results from literatures.

Declaration of Competing Interest

The authors declare that they have no known competing financial interests or personal relationships that could have appeared to influence the work reported in this paper.

Acknowledgments

The authors gratefully acknowledge the financial support from the Independent Research Fund

Denmark (DFF) and MAN Energy Solutions under the grant number 8022-00143B. The computation was performed using the Niflheim cluster at the Technical University of Denmark (DTU).

Supplementary material

Supplementary material associated with this article can be found, in the online version, at doi:10.1016/j.proci.2020.08.018

References

[1] M.K. Bobba, C.L. Genzale, M.P. Musculus, *SAE International Journal of Engines* 2 (1) (2009) 911–924.
[2] A.G. Erman, P. Hellier, N. Ladommatos, *Fuel* (2019).
[3] P. Bergstrand, I. Denbratt, Diesel combustion with reduced nozzle orifice diameter (2001).
[4] D. Nikolic, K. Wakimoto, S. Takahashi, N. Iida, Effect of nozzle diameter and EGR ratio on the flame temperature and soot formation for various fuels(2001).
[5] B.-S. Kim, W.H. Yoon, S.H. Ryu, J.S. Ha, Effect of the injector nozzle hole diameter and number on the spray characteristics and the combustion performance in medium-speed diesel marine engines (2005).
[6] P. Roels, Y. Sledsens, S. Verhelst, R. Sierens, L. Vervaeke, Reducing engine-out emissions for medium high speed diesel engines: influence of injection parameters (2009).
[7] X. Wang, Z. Huang, W. Zhang, O.A. Kuti, K. Nishida, *Applied Energy* 88 (5) (2011) 1620–1628.
[8] D. Siebers, B. Higgins, *SAE Transactions, 2001-01-0530* (2001) 400–421.
[9] Engine combustion network, 2019, https://ecn.sandia.gov/.
[10] F. Westlye, *Experimental Study of Liquid Fuel Spray Combustion*, Technical University of Denmark (DTU), 2016.
[11] J.V. Pastor, J.M. Garcia-Oliver, A. Garcia, A.M. López, An experimental investigation on spray mixing and combustion characteristics for Spray C/D nozzles in a constant pressure vessel (2018).
[12] K.M. Pang, M. Jangi, X.-S. Bai, J. Schramm, J.H. Walther, *Energy Procedia* 142 (2017) 1028–1033 .
[13] J.M. Desantes, J.M. García-Oliver, R. Novella, L. Pachano, *International Journal of Engine Research* (2019).
[14] Y. Pei, S. Som, E. Pomraning, P.K. Senecal, S.A. Skeen, J. Manin, L.M. Pickett, *Combustion and Flame* 162 (12) (2015) 4442–4455.
[15] K.M. Pang, M. Jangi, X.-S. Bai, J. Schramm, J.H. Walther, *Combustion and Flame* 193 (2018) 363–383.
[16] R.D. Reitz, R. Diwakar, *SAE Transactions, 870598* (1987) 492–509.
[17] T. Yao, Y. Pei, B.-J. Zhong, S. Som, T. Lu, K.H. Luo, *Fuel* 191 (2017) 339–349.
[18] P.C. Ma, H. Wu, T. Jaravel, L. Bravo, M. Ihme, *Proceedings of the Combustion Institute* 37 (3) (2019) 3303–3310.
[19] H. Kahila, A. Wehrfritz, O. Kaario, V. Vuorinen, *Combustion and Flame* 199 (2019) 131–151.
[20] H. Kahila, A. Wehrfritz, O. Kaario, M.G. Masouleh, N. Maes, B. Somers, V. Vuorinen, *Combustion and Flame* 191 (2018) 142–159.
[21] C.K. Blomberg, L. Zeugin, S.S. Pandurangi, M. Bolla, K. Boulouchos, Y.M. Wright, *SAE International Journal of Engines* 9 (4) (2016) 2107–2119.
[22] J. Chomiak, A. Karlsson, *Symposium (International) on Combustion* 26 (2) (1996) 2557–2564.
[23] M. Jangi, R. Yu, X.-S. Bai, *Flow, Turbulence and Combustion* 90 (2) (2013) 285–299.
[24] A. Hadadpour, M. Jangi, K.M. Pang, X.S. Bai, *Proceedings of the Combustion Institute* 37 (4) (2019) 4709–4716.
[25] M. Jangi, R. Solsjo, B. Johansson, X.-S. Bai, *International Journal of Heat and Fluid Flow* 53 (2015) 68–80.
[26] A. Wehrfritz, V. Vuorinen, O. Kaario, M. Larmi, *Atomization and Sprays* 23 (5) (2013).
[27] N. Maes, M. Meijer, N. Dam, B. Somers, H.B. Toda, G. Bruneaux, S.A. Skeen, L.M. Pickett, J. Manin, *Combustion and Flame* 174 (2016) 138–151.
[28] C.K. Westbrook, *Proceedings of the Combustion Institute* 28 (2) (2000) 1563–1577.
[29] P. Kundu, M.M. Ameen, S. Som, *Combustion and Flame* 183 (2017) 283–298.
[30] A. Krisman, E.R. Hawkes, J.H. Chen, *Proceedings of the Combustion Institute* 37 (4) (2019) 4787–4795.
[31] G. Borghesi, A. Krisman, T. Lu, J.H. Chen, *Combustion and Flame* 195 (2018) 183–202.